J Mater Sci (2007) 42:9205–9209
DOI 10.1007/s10853-007-1887-0

A facile two-step hydrothermal route for the synthesis of γ-Fe_2O_3 nanocrystals and their magnetic properties

Hongliang Zhu · Deren Yang · Luming Zhu · Hong Yang · Dalai Jin · Kuihong Yao

Received: 28 January 2007 / Accepted: 29 May 2007 / Published online: 27 July 2007

Abstract This paper proposes a facile two-step hydrothermal route for the synthesis of maghemite (γ-Fe_2O_3) nanocrystals. The synthesis route included two steps: (i) hydrothermal synthesis of Fe_3O_4 nanocrystals, and (ii) hydrothermal oxidation of the Fe_3O_4 nanocrystals to their γ-Fe_2O_3 counterpart. Phase transition from γ-Fe_2O_3 to hematite was studied by in situ XRD; the γ-Fe_2O_3 nanocrystals exhibited enhanced phase transition temperature (>600 °C). The magnetization curves revealed that the γ-Fe_2O_3 nanocrystals showed ferromagnetic behavior with high saturation magnetization of 68 emu/g at room temperature.

Introduction

Iron(III) oxide has four polymorphs, namely, hematite (α-Fe_2O_3), maghemite (γ-Fe_2O_3), β-Fe_2O_3 and ε-Fe_2O_3 [1]. Among these polymorphs, γ-Fe_2O_3 is an excellent ferromagnetic oxide that has been widely used as magnetic recording materials for the long period of time [2, 3]. As the density of magnetic recording media increases, it is technologically important to study the synthesis and properties of γ-Fe_2O_3 nanocrystals. In addition, nanocrystalline γ-Fe_2O_3 has promising applications in ferrofluids [4, 5], magnetic refrigeration [6], magneto-optical devices [7], controlled drug delivery [8], bioprocessing [1, 9], medical diagnosis [10, 11], and gas sensors [12]. Due to the chemical stability, biocompatibility and heating ability of γ-Fe_2O_3 nanocrystals in an alternating field, ferrofluids of γ-Fe_2O_3 nanocrystals also can be used for magnetic fluid hyperthermia (MFH) in tumour treatments [13, 14].

The usual technique to synthesize γ-Fe_2O_3 powders is still the thermal oxidation of magnetite (Fe_3O_4), which includes two steps. First, Fe_3O_4 powders are synthesized by coprecipitation of ferrous and ferric cations in alkaline solution. Then, the Fe_3O_4 powders are oxidized to their γ-Fe_2O_3 counterpart between 100 °C and 250 °C in air. In recent years, a variety of processes have been employed to prepare γ-Fe_2O_3 nanocrystals, including solvothermal reduction [15], thermal decomposition [16], reduction–oxidation method [17], high temperature aging methods [18], ball-milling [19], coprecipitation technique [20], reverse micelle technique [21], sol–gel mediated reaction [22] and so on.

Hydrothermal method is a powerful technique in synthesizing metal oxide nanostructures, but hydrothermal synthesis of γ-Fe_2O_3 nanocrystals is still less successful. In usual hydrothermal processes, nanocrystalline hematite (α-Fe_2O_3) instead of γ-Fe_2O_3 can be obtained because α-Fe_2O_3 is the most thermodynamically stable ferric oxide [23, 24]. Chen and Xu have reported that γ-Fe_2O_3 nanoparticles could be hydrothermally synthesized at 140 °C for 7–10 days using 2-methoxyethanol (MOE)-H_2O mixed solvent and acetylacetone(Hacac) as additive from iron(II) 2-methoxyethoxides ($Fe(MOEO)_2$) [25]. However, this hydrothermal synthesis process is troublesome. In contrast, hydrothermal synthesis of Fe_3O_4 nanocrystals have been reported by many literatures [26–30]. Considering the above points, we propose in this paper a facile two-step

H. Zhu · D. Yang (✉)
State Key Lab of Silicon Materials, Zhejiang University, Hangzhou 310027, P.R. China
e-mail: mseyang@zju.edu.cn

H. Zhu (✉) · L. Zhu · H. Yang · D. Jin · K. Yao
Center of Materials Engineering, Zhejiang Sci-Tech University, Xiasha University Town, Hangzhou 310018, P.R. China
e-mail: zhuhl@zstu.edu.cn

hydrothermal route for the synthesis of γ-Fe_2O_3 nanocrystals, which includes hydrothermal synthesis of Fe_3O_4 nanocrystals using hydrazine hydrate as an alkaline mineralizer and subsequent hydrothermal oxidation of the Fe_3O_4 nanocrystals to its γ-Fe_2O_3 counterpart.

Experimental procedure

The starting reagents used in this work were analytical-grade ferrous sulfate hydrate ($FeSO_4{\cdot}7H_2O$), hydrazine hydrate 85% and hydrogen peroxide (H_2O_2) with a volume concentration of 30%. At the first stage, 1.779 g of $FeSO_4{\cdot}7H_2O$ and 0.753 g of hydrazine hydrate 85% were added to 160 mL of deionized water under vigorous magnetic stirring. After 10 min of stirring, the above solution was transferred into a Teflon-lined stainless steel autoclave (capacity 200 ml) and sealed. The autoclave was heated at 150 °C for 12 h and then cooled down naturally to room temperature. The black Fe_3O_4 nanocrystals was collected by centrifugation. At the second stage, the Fe_3O_4 nanocrystals, 10 ml of H_2O_2 and 150 ml of deionized water were introduced into the Teflon-lined stainless steel autoclave and sealed. Once again, the autoclave was heated at 150 °C for 12 h and then cooled down naturally to room temperature. Finally, the brown γ-Fe_2O_3 nanocrystals were collected by centrifugation and washing with distilled water and alcohol for several times, and dried at 60 °C for 24 h in air.

Phase identification of the products was carried out by x-ray diffraction (XRD) using a Thermo ARL XTRA x-ray diffractometer with Cu Kα radiation (λ = 1.54178 Å). The chemical compositions of the Fe_3O_4 and γ-Fe_2O_3 nanocrystals were analyzed by an Oxford Instrument's INCA energy-dispersive spectrometer (EDS). In situ high-temperature XRD study of the $\gamma \rightarrow \alpha$-$Fe_2O_3$ phase transition was performed in a high-temperature attachment of the x-ray diffractometer. The sample was placed on a Pt stage and heated in air. In situ XRD patterns were obtained at different temperatures, i.e. 30, 100, 200, 300, 400, 500, 600, 650, 700, 750 and 800 °C. XRD scanning was started when the sample was heated at a temperature for 20 min. The morphologies of the Fe_3O_4 and γ-Fe_2O_3 nanocrystals were observed by a JEOL JEM 200 CX transmission electron microscope (TEM) operated at 160 kV. The magnetic properties were measured on a Quantum Design Physical Property Measurement System (PPMS-9).

Results and discussion

The black product hydrothermally synthesized at the first step and the brown product hydrothermally oxidized at the second step were characterized by XRD. Their XRD patterns are shown in Figs. 1a, b, respectively. Analyzed by the Thermo ARL WinXRD software package, all the peaks of the XRD pattern of the black product (shown in Fig. 1a) are in good agreement with the JCPDS data (no. 79-0419) of the cubic Fe_3O_4 with the lattice constant a = 8.40 Å. The brown product can be indexed to cubic γ-Fe_2O_3 (JCPDS no. 39-1346) with the lattice constant a = 8.35 Å. No XRD peaks of impurities such as α-Fe_2O_3 phase were found in Fig. 1b. Maghemite with cubic structure is closely related to the structure of inverse spinel Fe_3O_4, but it differs from the latter by the presence of vacancies distributed on the cation sublattice [31]. The Fe_3O_4 and γ-Fe_2O_3 nanocrystals, consequently, show almost similar XRD patterns (see Fig. 1). Fortunately, modern high-resolution x-ray diffractometers have enough high precision to distinguish between Fe_3O_4 and γ-Fe_2O_3. The inset of Fig. 1 clearly shows the amplified (511) and (440) peaks of the Fe_3O_4 and γ-Fe_2O_3 nanocrystals, in which obvious peak difference can be found. In addition, the chemical compositions of the Fe_3O_4 and γ-Fe_2O_3 nanocrytals were analyzed by EDS. Their EDS spectra and results of quantitative analysis by the Oxford Instruments INCA software package (INCA Energy 200) are shown in Fig. 2a and b, respectively. As shown in Fig. 2, strong peaks for Fe and O can be found in the spectra. The results of quantitative analysis (see the insets of Fig. 2) reveals that the O/Fe atomic ratios of the Fe_3O_4 and γ-Fe_2O_3 nanocrytals are 1.30 and 1.52, respectively. The values are consistent

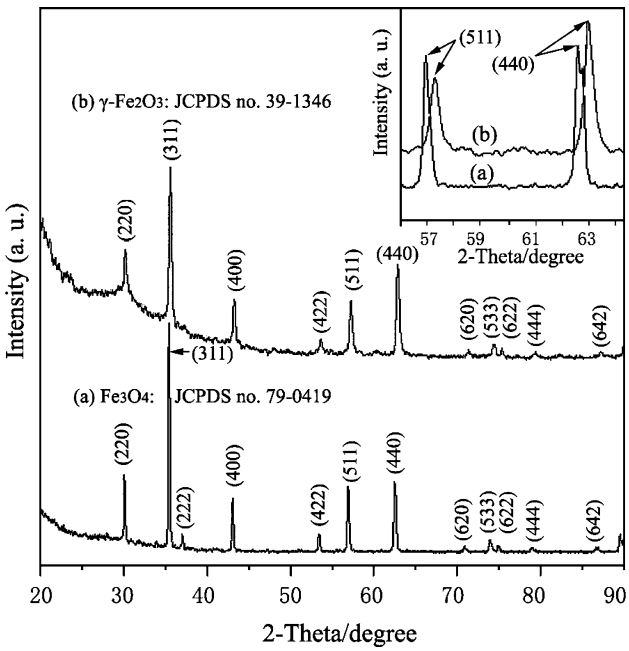

Fig. 1 XRD patterns of the products: (**a**) Fe_3O_4 nanocrystals, and (**b**) γ-Fe_2O_3 nanocrystals

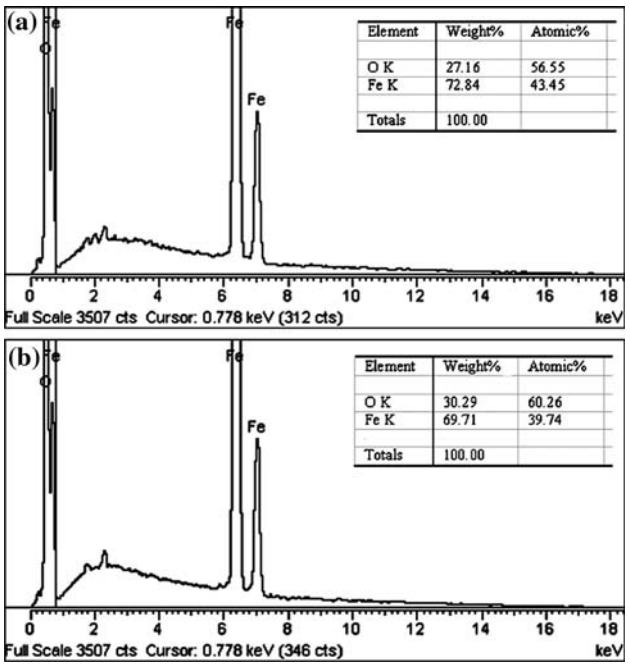

Fig. 2 EDS spectra and results of quantitative analysis: (**a**) Fe_3O_4 nanocrystals, and (**b**) γ-Fe_2O_3 nanocrystals

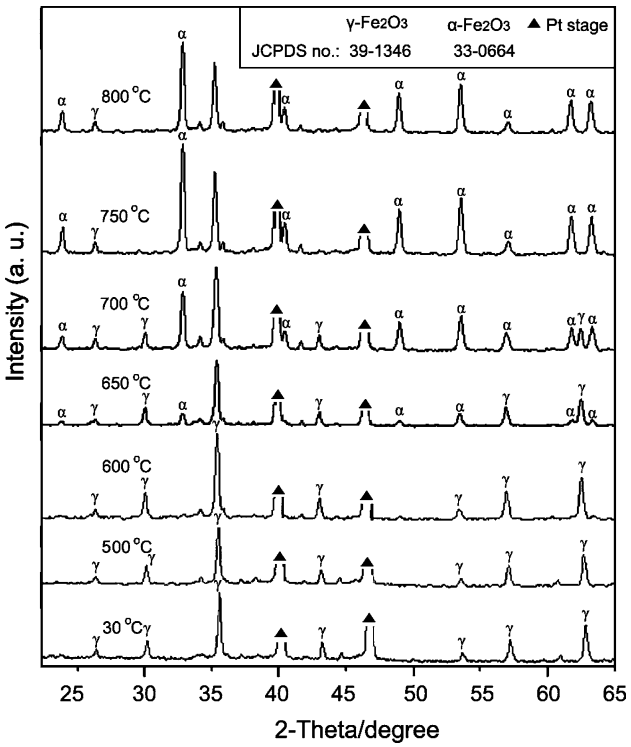

Fig. 3 In situ XRD patterns of the phase transition from maghemite (γ-Fe_2O_3) to hematite (α-Fe_2O_3)

with the theoretical O/Fe atomic ratios of Fe_3O_4 (1.33) and γ-Fe_2O_3 (1.50). In a word, the black and brown products were Fe_3O_4 and γ-Fe_2O_3, respectively.

It is well known that cubic γ-Fe_2O_3 is only a metastable, low temperature Fe_2O_3 modification and that the phase transition to rhombohedral α-Fe_2O_3 occurs at temperature range of 200–700 °C [32–34]. To meet technological challenges for memory devices, the enhanced phase transition temperature implies better applicability of γ-Fe_2O_3 even at high temperature. There have been many efforts to stabilize γ-Fe_2O_3 against transformation to α-Fe_2O_3 at enhanced temperatures [34–36]. In contrast to other thermal analysis techniques such as DSC, DTA and TGA, in situ XRD is a more powerful tool to study phase transition. In this work, the $\gamma \rightarrow \alpha$-$Fe_2O_3$ phase transition was studied by in situ XRD. Figure 3 shows the in situ XRD patterns obtained at 30, 500, 600, 650, 700, 750 and 800 °C . As shown in Fig. 3, no XRD peaks of α-Fe_2O_3 were detected in the temperature range of 30–600 °C. When the γ-Fe_2O_3 sample was heated to 650 °C, the XRD peaks of α-Fe_2O_3 (JCPDS no. 33-0664) began to occur. Furthermore, the XRD peaks of the α-Fe_2O_3 became stronger and stronger with increasing temperature. For instance, the (104) peak at around 33.1°, the strongest peak in the standard card of α-Fe_2O_3 (JCPDS no. 33-0664) didn't occure until the γ-Fe_2O_3 sample was heated to 650 °C. In subsequent heating to 800 °C, the (104) peak became increasingly strong, meaning the phase transition was induced. Based on above results, it can been concluded that the γ-Fe_2O_3 nanocrytals synthesized via the two-step hydrothermal route exhibited high phase transition temperature (>600 °C), while the reported temperature of the $\gamma \rightarrow \alpha$-$Fe_2O_3$ transition ranges from 200 C to 500 °C for nanoparticles [32]. We attributed the high transition temperature (>600 °C) to the particular hydrothermal oxidation process.

The morphologies of the Fe_3O_4 and γ-Fe_2O_3 nanocrystals were observed by TEM; their typical TEM images are shown in Fig. 4. Figure 4a shows the TEM image of the black Fe_3O_4 product, which reveals that the product is Fe_3O_4 nanocrystals with the diameter of ~70 nm. The TEM images of the γ-Fe_2O_3 product are shown in Figs. 4b, c, which reveal that the γ-Fe_2O_3 product has the same morphology as that of the Fe_3O_4 nanocrystals. The inset of Fig. 4c shows the selected area electron diffraction (SAED) pattern of the γ-Fe_2O_3 nanocrystals. The d values corresponding to the two brightest rings (from the inner to the outer) are 2.10 Å and 1.28 Å, corresponding well to the {400} and {533} planes of the γ-Fe_2O_3 (JCPDS no. 39-1346), respectively. Furthermore, as shown in Fig. 4, the Fe_3O_4 and γ-Fe_2O_3 nanocrystals are well dispersive.

The magnetization curves of the Fe_3O_4 and γ-Fe_2O_3 nanocrystals are shown in Fig. 5. The related magnetic parameters are given in Table 1. As shown in Fig. 4, their magnetization curves measured at both 10 K and 300 K exhibit obvious hysteresis loop. The hysteresis loops is the

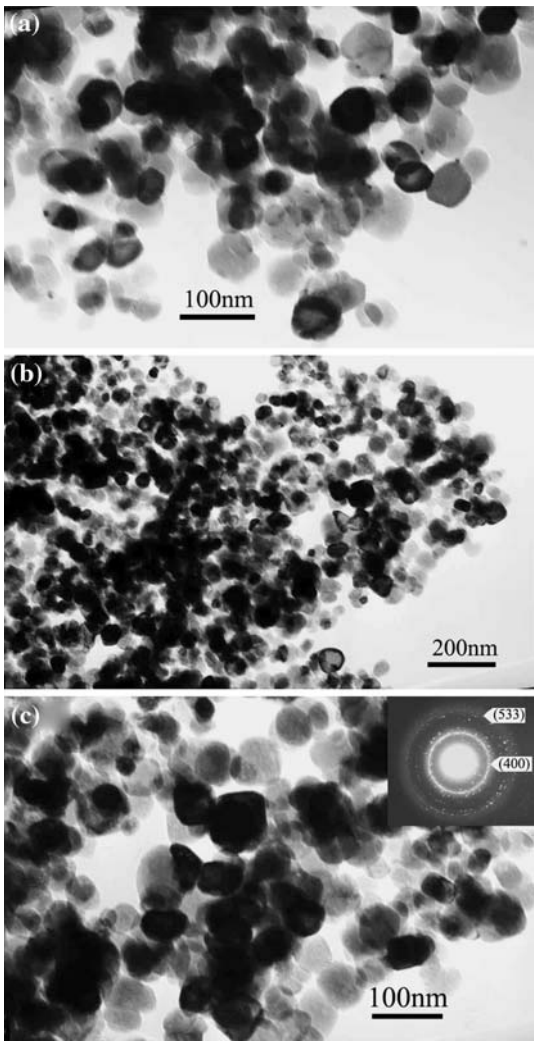

Fig. 4 (**a**) TEM image of the Fe_3O_4 nanocrystals, (**b**) the low-magnification TEM image of γ-Fe_2O_3 nanocrystals, and (**c**) the magnified TEM image of the γ-Fe_2O_3 nanocrystals, the inset is the relative SEAD pattern

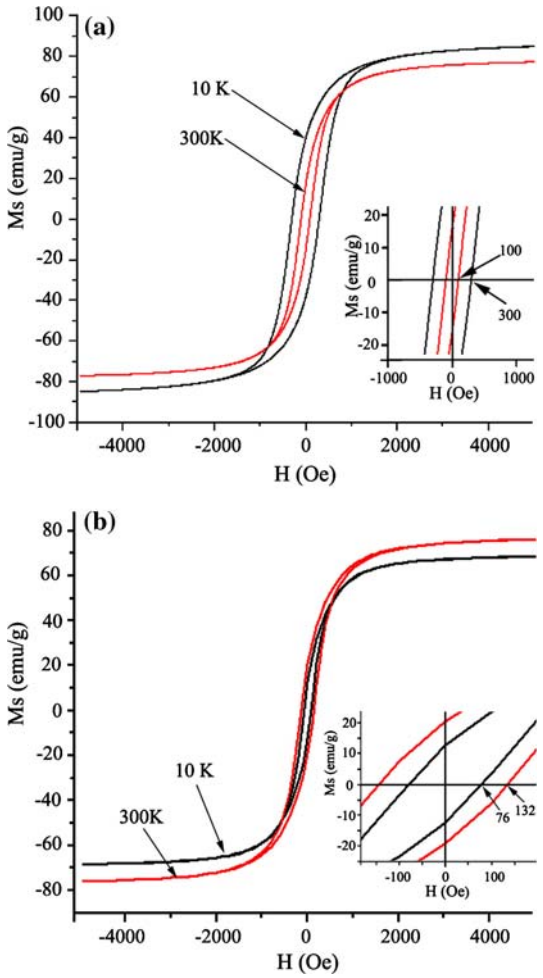

Fig. 5 Magnetization curves of the products measured at 10 K and 300 K: (**a**) Fe_3O_4 nanocrystals, and (**b**) γ-Fe_2O_3 nanocrystals

unique characteristic of the ferromagnetic behavior, meaning that the Fe_3O_4 and γ-Fe_2O_3 nanocrystals show typical ferromagnetic behavior at 10 Kand 300 K. Due to their high crystallinity, the γ-Fe_2O_3 nanocrystals show high saturation magnetization of 68 emu/g at 300 K, which is close to the theoretical saturation magnetization of 76 emu/g for bulk γ-Fe_2O_3 at room temperature [37].

Table 1 Magnetic properties of the Fe_3O_4 and γ-Fe_2O_3 nanocrystals obtained with the PPMS

Product	Measuring temp. (K)	Saturation magnetization (emu/g)	Coercivity (Oe)
Fe_3O_4	10	85	300
	300	77	100
γ-Fe_2O_3	10	76	132
	300	68	76

Note: The masses of the Fe_3O_4 and γ-Fe_2O_3 samples measured with the PPMS are 8.0 and 82.4 mg, respectively

Conclusions

Maghemite (γ-Fe_2O_3) nanocrystals were successfully prepared via a facile two-step hydrothermal route. The synthesis route includes two steps: (i) hydrothermal synthesis of Fe_3O_4 nanocrystals, and (ii) hydrothermal oxidation of the Fe_3O_4 nanocrystals to its γ-Fe_2O_3 counterpart. The γ-Fe_2O_3 nanocrystals were well-crystallized and about 70 nm in diameter. In situ XRD study reveals the γ-Fe_2O_3 nanocrystals exhibit the enhanced phase transition temperature (>600 °C). The γ-Fe_2O_3 nanocrystals show ferromagnetic behavior with high saturation magnetization of 68 emu/g at room temperature.

Acknowledgments This work was supported by the Open Foundation Project of the State Key Lab of Silicon Materials (No. 200601). We also thank Prof Chunmu Feng (Zhejiang University) for PPMS measurements.

References

1. Zboril R, Mashlan M, Petridis D (2002) Chem Mater 14:969
2. Osmond WP (1952) Proc Phys Soc Lond B65:121
3. Osmond WP (1953) Proc Phys Soc Lond B66:265
4. Yu L, Yin Y, Mayers BT, Xia Y (2002) Nano Lett 2:183
5. Buioca CD, Iusan V, Stanci A, Zoller C (2002) J Magn Magn Mater 252:318
6. Tartaj P, Serna CJ (2002) Chem Mater 14:4396
7. Ortega D, Garitaonandia JS, Barrera-Solano C, Ramírez-del-Solar M, Blanco E, M Domínguez (2006) J Non-Cryst Solids 352:2801
8. Xu Z, Zeng Q, Lu G, Yu A (2006) Chem Eng Sci 61:1027
9. Bhatnagar SP, Rosensweig RE (1995) J Magn Magn Mater 149:198
10. Gupta AK, Gupta M (2005) Biomaterials 26:3995
11. Lu J, Yang S, Ng KM, Su CH, Yeh CS, Wu YN, Shieh DB (2006) Nanotechnology 17:5812
12. Jing Z, Wang Y, Wu S (2006) Sensor Actuat B Chem 113:177
13. Jordan A, Scholz R, Wust P, Schirra H, Schiestel T, Schmidt H, Felix R (1999) J Magn Magn Mater 194:185
14. Chan DCF, Kirpotin DB, Bunn JPA (1993) J Magn Magn Mater 122:374
15. Liu X, Fu S, Xiao H (2006) J Solid State Chem 179:1554
16. Rockenberger J, Scher EC, Alivisatos AP (1999) J Am Chem Soc 121:11595
17. Ni Y, Ge X, Zhang Z, Ye Q (2002) Chem Mater 14:1048
18. Hyeon T, Lee SS, Park J, Chung Y, Na B (2001) J Am Chem Soc 123:12798
19. Janot R, Guérard D (2002) J Alloy Comp 333:302
20. Lee S, Jeong J, Shin S, Kim J, Kim J (2004) J Magn Magn Mater 282:147
21. Mukadam MD, Yusuf SM, Sharma P, Kulshreshtha SK (2004) J Magn Magn Mater 272–276:1401
22. Woo K, Lee JHJ (2004) J Magn Magn Mater 272–276:e1155
23. Giri S, Samanta S, Maji S, Ganguli S, Bhaumik A (2005) J Magn Magn Mater 285:296
24. Kandori K, Ishikawa T (2004) J Colloid Interf Sci 272:246
25. Chen D, Xu R (1998) J Solid State Chem 137:185
26. Wang J, Sun J, Chen Q (2003) Mater Res Bull 38:1113
27. Lian S, Kang Z, Wang E, Jiang M, Hu C, Xu L (2003) Solid State Commun 127:605
28. Zheng Y, Cheng Y, Bao F, Wang Y (2006) Mater Res Bull 41:525
29. Wan J, Chen X, Wang Z, Yang X, Qian Y (2005) J Cryst Growth 276:571
30. Xuan S, Hao L, Jiang W, Gong X, Hu Y, Chen Z (2007) J Magn Magn Mater 308:210
31. Belin T, Guigue-Millot N, Caillot T, Aymes D, Niepce JC (2002) J Solid State Chem 163:459
32. Ennas G, Marongiu G, Musinu A, Falqui A, Ballirano P, Caminiti R (1999) J Mater Res 14:1570
33. Clark SM, Prilliman SG, Erdonmez CK, Alivisatos AP (2005) Nanotechnology 16:2813
34. Gnanaprakash G, Ayyappan S, Jayakumar T, Philip J, Raj B (2006) Nanotechnology 17:5851
35. Berry FJ, Greaves C, Helgason O, McManus J (1999) J Mater Chem 9:223
36. Lai J, Shafi KVPM, Loos K, Ulman A, Lee, Vogt T, Estournes C (2003) J Am Chem Soc 125:11470
37. Cullity BD (1972) Introduction to magnetic materials reading. Addison-Wesley, MA